

This is an electronic reprint of the original article. This reprint may differ from the original in pagination and typographic detail.

---

## Comprehensive Studies on the Role of Small Aliphatic Alcohols in the Direct Synthesis of Hydrogen Peroxide with a Combination of Solvent Step and In Situ FTIR-ATR Experiments

Reinsdorf, O; Eränen, K; Salmi, T

*Published in:*  
Catalysts

*DOI:*  
[10.3390/catal13040753](https://doi.org/10.3390/catal13040753)

Published: 14/04/2023

*Document Version*  
Final published version

*Document License*  
CC BY

[Link to publication](#)

*Please cite the original version:*

Reinsdorf, O., Eränen, K., & Salmi, T. (2023). Comprehensive Studies on the Role of Small Aliphatic Alcohols in the Direct Synthesis of Hydrogen Peroxide with a Combination of Solvent Step and In Situ FTIR-ATR Experiments. *Catalysts*, 13(4), Article 753. <https://doi.org/10.3390/catal13040753>

### General rights


Copyright and moral rights for the publications made accessible in the public portal are retained by the authors and/or other copyright owners and it is a condition of accessing publications that users recognise and abide by the legal requirements associated with these rights.

### Take down policy

If you believe that this document breaches copyright please contact us providing details, and we will remove access to the work immediately and investigate your claim.

## Article

# Comprehensive Studies on the Role of Small Aliphatic Alcohols in the Direct Synthesis of Hydrogen Peroxide with a Combination of Solvent Step and In Situ FTIR-ATR Experiments

Ole Reinsdorf <sup>\*</sup> , Kari Eränen and Tapio Salmi

Laboratory for Industrial Chemistry and Reaction Engineering (TKR), Åbo Akademi, Henrikinkatu 2, 20500 Turku, Finland

<sup>\*</sup> Correspondence: ole.reinsdorf@abo.fi

**Abstract:** A combination of transient methods in a laboratory-scale trickle bed reactor and attenuated total reflection (ATR)-infrared spectroscopy was applied to gain insight into the reaction mechanism of the direct synthesis of hydrogen peroxide (DSHP) on a commercial 5 %Pd/C catalyst, with water and methanol used as solvents. During the transient studies, after the switch from water to methanol, an oscillatory pattern was observed in which methoxy and hydroxymethyl species were observed prior to the peroxide species. From the specific position and the maxima in the intensities of these species over time, an augmented reaction scheme for the DSHP in methanol was proposed, in which methanol can form hydroxymethyl species which act as co-catalysts to reduce absorbed oxygen species.

**Keywords:** direct synthesis of hydrogen peroxide; transient studies; solvent effect; in situ FTIR-ATR



**Citation:** Reinsdorf, O.; Eränen, K.; Salmi, T. Comprehensive Studies on the Role of Small Aliphatic Alcohols in the Direct Synthesis of Hydrogen Peroxide with a Combination of Solvent Step and In Situ FTIR-ATR Experiments. *Catalysts* **2023**, *13*, 753. <https://doi.org/10.3390/catal13040753>

Academic Editor: Giuseppe Bonura

Received: 17 March 2023

Revised: 12 April 2023

Accepted: 13 April 2023

Published: 14 April 2023



**Copyright:** © 2023 by the authors. Licensee MDPI, Basel, Switzerland. This article is an open access article distributed under the terms and conditions of the Creative Commons Attribution (CC BY) license (<https://creativecommons.org/licenses/by/4.0/>).

## 1. Introduction

Hydrogen peroxide is widely considered to be a promising and green oxidant because it produces only water as a stoichiometric co-product and thus avoids toxic waste. The current industrial method of producing hydrogen peroxide is the anthraquinone process in which 2-alkyl-anthraquinone is first reduced to 2-alkyl-anthrahydroquinone [1]. In consecutive steps, the latter is re-oxidized while producing hydrogen peroxide. The process is cumbersome and involves the recirculation of the working solution in which by-products and impurities are accumulated. The anthraquinone process is profitable only in very large production scales.

As an alternative, the direct synthesis of hydrogen peroxide (DSHP) can be achieved from hydrogen and oxygen in green solvents such as water and alcohols. In recent years, extensive research efforts have been devoted to direct synthesis, from catalysts to kinetics, reactors and process concepts. Palladium and gold are catalytically active metals in direct synthesis. Through direct synthesis, it is possible to reduce the cost of separation, as well as lowering the overall energy consumption [2–5]. The mechanism for this reaction does not follow a classical Langmuir–Hinshelwood model. Instead, it has been shown to work similarly to an oxygen reduction reaction (ORR), as reported by Wilson and Flaherty [6,7]. In this mechanism, they propose that a proton–electron transfer takes place to reduce the oxygen.

A major role in the reaction is played by the selected liquid phase [8–10]. It has been shown by several groups that the reaction can only proceed in protic solvents such as alcohols and water. In aprotic solvents, the reaction does not take place. Even in protic solvents, the choice of solvent has a major influence on the yield of hydrogen peroxide and selectivity. In an aqueous environment, significantly lower concentrations of hydrogen peroxide are obtained, compared to alcohols. This has been traditionally regarded as a result of the higher gas solubilities in organic solvents [8,10,11]. However, it has been

shown that the reaction shows a first-order dependency on the hydrogen and a zero-order dependency on the oxygen partial pressure in ethanol [12,13] and methanol [6], in contrast to the first-order dependency it has on both reaction gases in water. This stands in contrast to the earlier findings of our group [14,15], wherein first-order kinetics were found for both reactants. Additionally, this observation cannot be explained by the higher solubility, but suggests the participation of the protic solvent in the reaction itself.

Based on these results and in order to further elucidate the mechanism of direct synthesis, we applied transient techniques in a laboratory-scale trickle bed reactor (TBR), which has previously turned out to be a potent reactor set-up for the DSHP [16–18], to study the role of protic solvents in the DSHP. Transient methods have significant advantages in comparison to classical steady-state experiments. With steady-state experiments, it is possible to create a global reaction scheme and an overall rate equation. However, this only allows for limited access to elementary reaction steps on the surface of the heterogeneous catalyst. In contrast, by disturbing the steady state and measuring the response of the system after a step-change at the reactor inlet, it is possible to elucidate the reaction mechanism in a more detailed way. Transient experiments have mainly been applied for gas–solid or liquid–solid systems by changing, for example, the flow, temperature, concentration or isotopic distribution [19–22]. Nonetheless, it was possible to implement the transient method in the three-phase system by using alcohols as model compounds for protic solvents in DSHP. To achieve further knowledge and better understanding of which species in reality are involved in the reaction, FTIR-ATR experiments are applied in the present work. ATR as a spectroscopic method based on the use of infrared radiation is a powerful tool to gain insight in reaction mechanisms, due its high surface sensitivity. It is possible to detect surface intermediates on heterogeneous catalysts during the reaction. In contrast to diffusive reflectance infra red Fourier transformed spectroscopy (DRIFTS), however, it can be applied to three-phase systems [23].

## 2. Results and Discussion

### 2.1. Solvent Step Experiments in TBR

In all the solvent step experiments, it was found, in agreement with previous experiments from Wilson and Flaherty [6] and Biasi et al. [16–18], that after a switch to the alcohol mixture, an increased concentration of hydrogen peroxide was detected. The change of the solvent feed resulted in a sharp step-change in the methanol concentration, suggesting minimal axial dispersion and back-mixing in the catalyst bed. Based on this observation, we excluded the impact of flow dynamics on the shape of the step of the hydrogen peroxide concentration. To minimize the influence of internal mass transfer limitations on the pores of the catalyst particles, the catalyst was applied as a finely dispersed powder. The exclusion of internal mass transfer limitations for this catalyst has been shown previously in the work of Gemo et al. [14]. As a result, the shape of the concentration response is predominantly dependent on the intrinsic reaction steps. After the switch from water to methanol (Figure 1), we expected a step shape that follows a similar contour to that of the solvent step. However, the concentration profile of hydrogen peroxide started to undergo a pattern of two major maxima and two minor maxima, which are incorporated in an oscillatory pattern. The concentration pattern was repeated, but with a declining amplitude approaching a steady state. This behavior was reproducible, as reported in detail in the Supplementary Information.

The amplitude of the pattern as well as the relative positions of the concentration peaks after the change to methanol shifted with a change in the concentration, with the first maxima used as a reference. By lowering the concentration of methanol in the reaction mixture, the oscillation pattern was stretched, leading to a flattening of the pattern. The change in the relative position of the maxima is displayed in Figure 2. The height of the step differs significantly, ranging from around 1.7 up to 5 times the concentration of hydrogen peroxide reached in water. In contrast, the steady-state concentration only ranges from 1.5 to 2.3 times the maximum concentration of hydrogen peroxide reached in water. It

seems that the steady state cannot be influenced predominantly by the concentration of methanol used in the system. A similar effect was observed when changing the temperature (Figure 2). By lowering the temperature, a similar stretching as well as a lowering of the maximum amplitude to 2.7 at 10 °C, or 2.2 at 5 °C, was observed. This influence of the concentration of methanol on the length pattern indicates that the pattern is a direct result of the available methanol for the reaction. This is further suggested by the strong increase in the height of the maximum with increasing methanol concentration. The concentration dependency shows a strong parabolic shape. This cannot be explained by the higher solubility of the reaction gases in methanol, which would demand a linear increase in the amount of hydrogen peroxide produced. The steady state remained, besides small differences, without any major change.

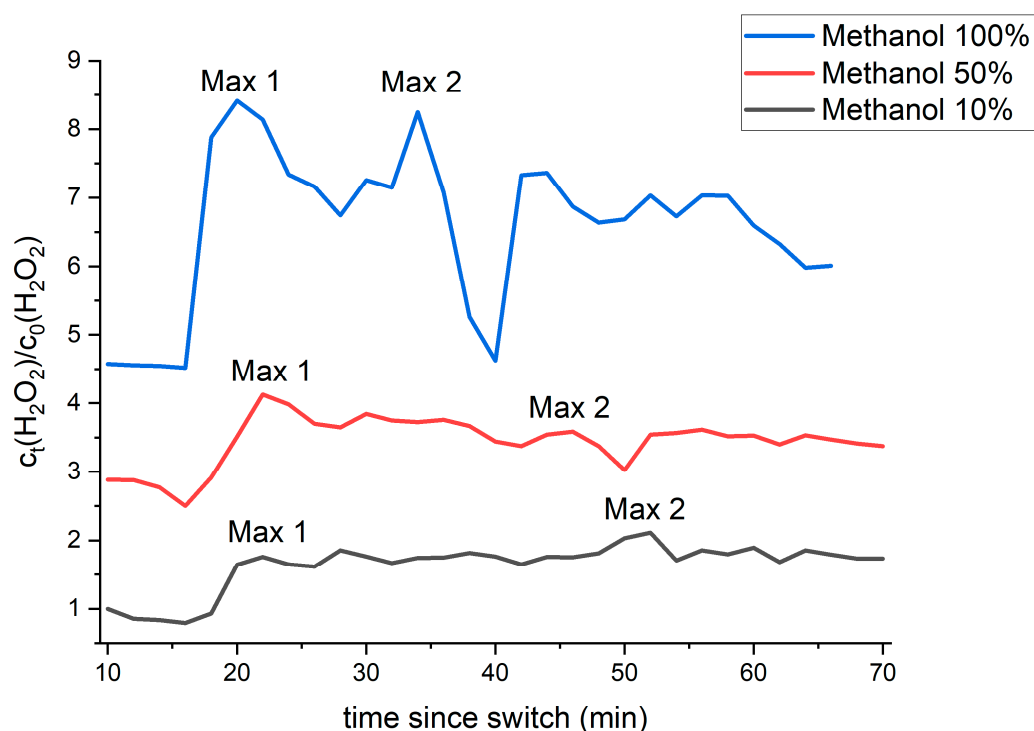


**Figure 1.** Relative transient response of ratio of hydrogen peroxide concentrations ( $\frac{c_{\text{measured}}}{c_{\text{steady state water}}}$ ), with a change in methanol concentration after the switch from water to different methanols ( $\vartheta = 15$  °C).

Even when using different alcohols, a similar dynamic pattern was observed. As seen in Figure 3, an increasing substitution of the hydroxylic carbon led to a proceeding separation of the first two and the two last maxima, or in case of 2-propanol, to a rapid decline in the concentration of hydrogen peroxide after the two first maxima. For the amplitude of the concentration pattern, no coherent trend could be found, so a decrease in the maximum amplitude from a factor of 5 to a factor of 3.1 in comparison to water was observed in ethanol. However, by shifting to 2-propanol, the factor measured levelled around 5.2 again. These observations suggest that at least two or more effects overlap each other. By using HPLC analysis, we observed additional signals which followed a similar pattern to the concentration of hydrogen peroxide, but with a phase delay. These signals could be attributed to formaldehyde and methyl formate when using methanol and acetaldehyde or acetone for ethanol and 2-propanol, respectively. Especially for 2-propanol, high concentrations of acetone were detected. The position of the maximum of the patterns of the dehydrogenation product at the same time as the dehydrogenation products reveals that their formation is directly related to the formation of hydrogen peroxide, since their concentration decrease rapidly after the concentration of hydrogen peroxide decreases.

Further, it indicates that under the conditions present at the time of the maximum, hydrogen peroxide favors the formation of dehydrogenation products.

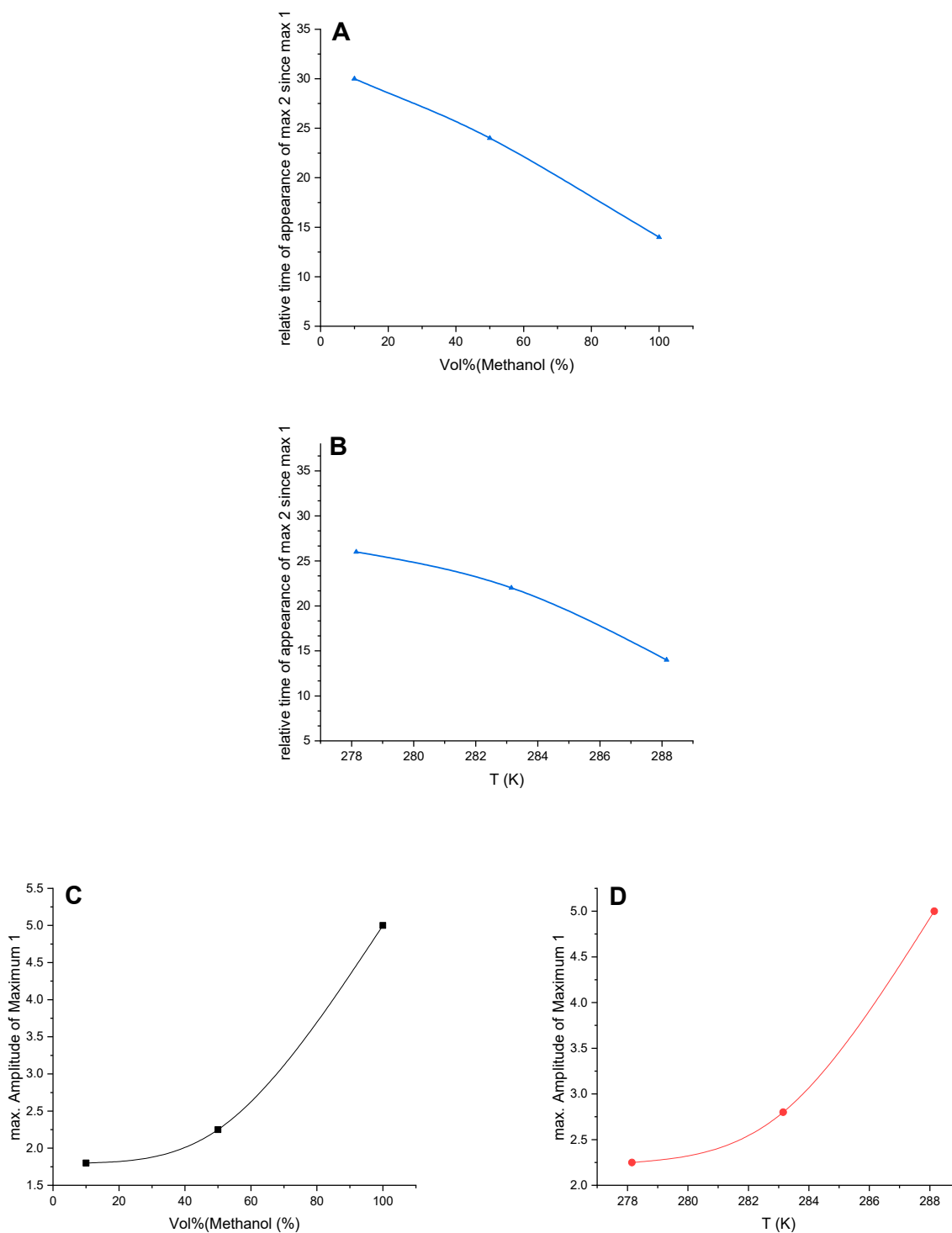


**Figure 2.** Concentration and temperature effects on the shape of the transient response. (A) relative times of the maxima in the hydrogen peroxide concentration at different methanol concentrations, (B) relative times of the maxima in the hydrogen peroxide concentration at different temperatures, (C) height of the first hydrogen peroxide maximum as function of methanol concentration, and (D) height of the first hydrogen peroxide maximum as function of temperature.

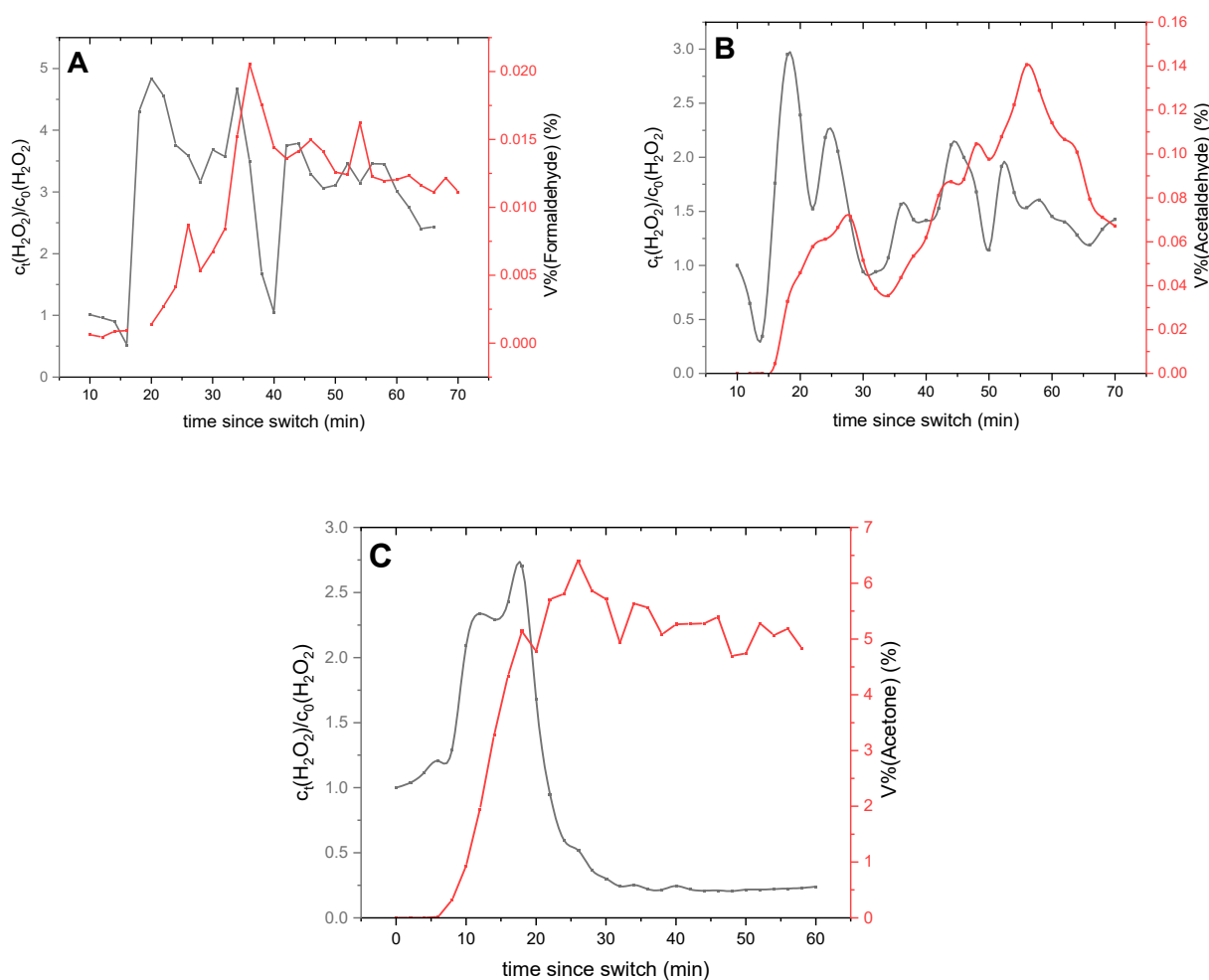


**Figure 3.** Relative transient response of ratio of hydrogen peroxide concentrations ( $\frac{c_{\text{measured}}}{c_{\text{steady state water}}}$ ) and the corresponding dehydrogenation of the products of alcohol ( $\vartheta = 15^\circ\text{C}$ ). (A) methanol, (B) ethanol, (C) iso-propanol.

## 2.2. Gas-Step Experiments

By changing the gas flows, we were able to see the dependencies of the concentrations on the reactants. Switching the gas flow from hydrogen to oxygen led to a small peak in the hydrogen peroxide concentration when the hydrogen flow was only applied with methanol, as illustrated in Figure 4. In contrast, a 100-fold higher concentration of hydrogen peroxide was observed after a switch from oxygen to hydrogen. This observation suggests a strong dependence of the reaction on the oxygen surface concentration. This was accompanied by a delayed peak of formaldehyde and methyl formate after the hydrogen peroxide peak in both cases. However, 10-fold higher concentrations of both dehydrogenation products are observed in the hydrogen-deficient environment, as observed after the switch from hydrogen to oxygen. Additionally, this observation in combination with the pattern observed in the solvent step experiments indicates the reason for the strong minimum in the transient oscillatory pattern observed. It can be concluded that the minimum in the hydrogen peroxide concentration is a result of strong hydrogen deficiency on the catalyst surface, as indicated by the high concentrations of dehydrogenation product. By varying the exposure time, no major changes in the peak shape were achieved.

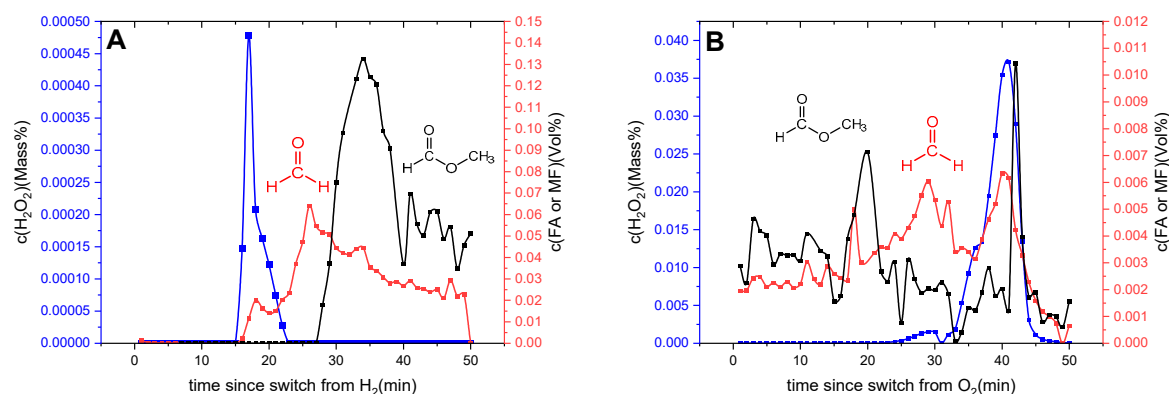


**Figure 4.** Transient responses of the hydrogen peroxide concentration, formaldehyde (FA) and methyl formate (MF) concentrations in methanol after the switch from (A) hydrogen-to-oxygen feed (B) oxygen-to-hydrogen feed.

### 2.3. Solvent Step Experiments in ATR

The response of the system after the change of solvent is displayed in Figure 2. Firstly, it is observed that the bands at  $1018\text{ cm}^{-1}$  ( $\nu(\text{C-O})$ ),  $2945\text{ cm}^{-1}$  ( $\nu(\text{C-H})$ ) and  $1450\text{ cm}^{-1}$ , assigned to methanol, rise steeply directly after the switch from water [24–26]. A similar but delayed rise was observed with the bands at  $3317\text{ cm}^{-1}$  [27,28] and  $3240\text{ cm}^{-1}$  [28,29]. These bands are attributed to the ( $\nu\text{O-H}$ ) vibration of the hydroxymethyl species and the peroxide species, respectively. At  $856\text{ cm}^{-1}$ , a small band was observed, which decreases in intensity after the switch but is recovered; this is the ( $\nu\text{O-O}$ ) vibration of adsorbed oxygen [29–33]. In addition, the vibrational band of methoxy species ( $1373\text{ cm}^{-1}$ ) slowly intensifies after methanol is applied [34,35]. Figure 5 depicts how the aforementioned band progresses over time after the switch to methanol (a series of full spectra is visible in the SI Figures S6 and S7). All of the observed bands are shown in Table 1.

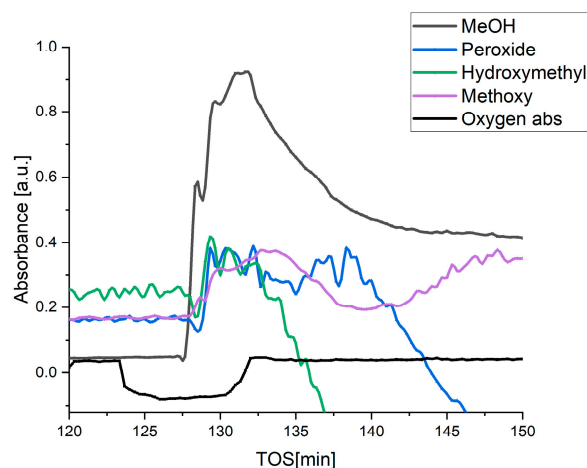


**Figure 5.** Evolution of the ATR spectra after the switch from water to methanol.

**Table 1.** Overview of important bands during the ATR experiments.

Band	Species	Frequency	Source
$\nu(\text{O-O})$	Oxygen (ads) <sup>a</sup>	$856\text{ cm}^{-1}$	[29–33]
$\nu(\text{C-O})$	Methanol	$1018\text{ cm}^{-1}$	[24–26]
$\nu(\text{CH}_3)$	Methoxy	$1373\text{ cm}^{-1}$	[34,35]
$\nu(\text{O-H})$	Hydroxymethyl	$3317\text{ cm}^{-1}$	[27,28]
$\nu(\text{O-H})$	Peroxide	$3240\text{ cm}^{-1}$	[28,29]

<sup>a</sup>—very weak.

As seen in the studies carried out in a laboratory scale trickle-bed-reactor, the transient response of the hydrogen peroxide concentration to this kind of solvent switch exhibited an oscillatory pattern in which the dehydrogenation products of methanol are found. In contrast to the large amplitude of the oscillation observed in the trickle bed reactor, the oscillations are smaller in amplitude, and no bands corresponding to formaldehyde species were detected. The pattern in which these oscillations appear in the ATR spectra shows that firstly, organic products, more specifically, methoxy species and hydroxymethyl species, emerge after the sharp edge of the band related to methanol and after the introduction of methanol into the system; then, the adsorbed oxygen and peroxide rise in intensity. On top of these oscillations, the different targeted bands show behaviors that are quite distinct from each other. It is evident that firstly, the hydroxymethyl and then methoxy species reach a maximum in intensity. This maximum of the methoxy species is meanwhile positioned in-between the two maxima of the peroxide concentration. After the sharp drop due to the choice of water as baseline, the band attributed to the hydroxymethyl species rises again slightly and achieves a stable level of absorbance. This happens after the second peroxide peak, as seen in Figure 6.

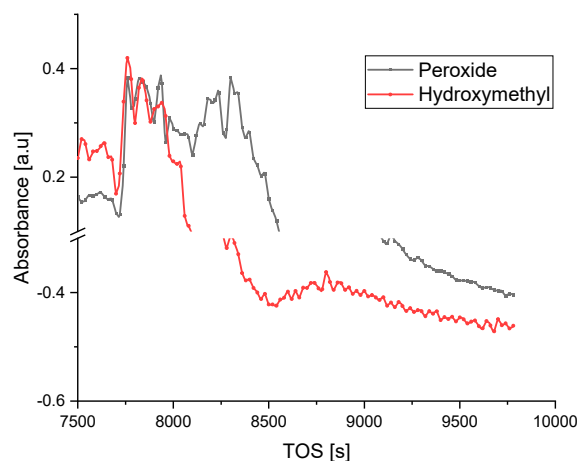


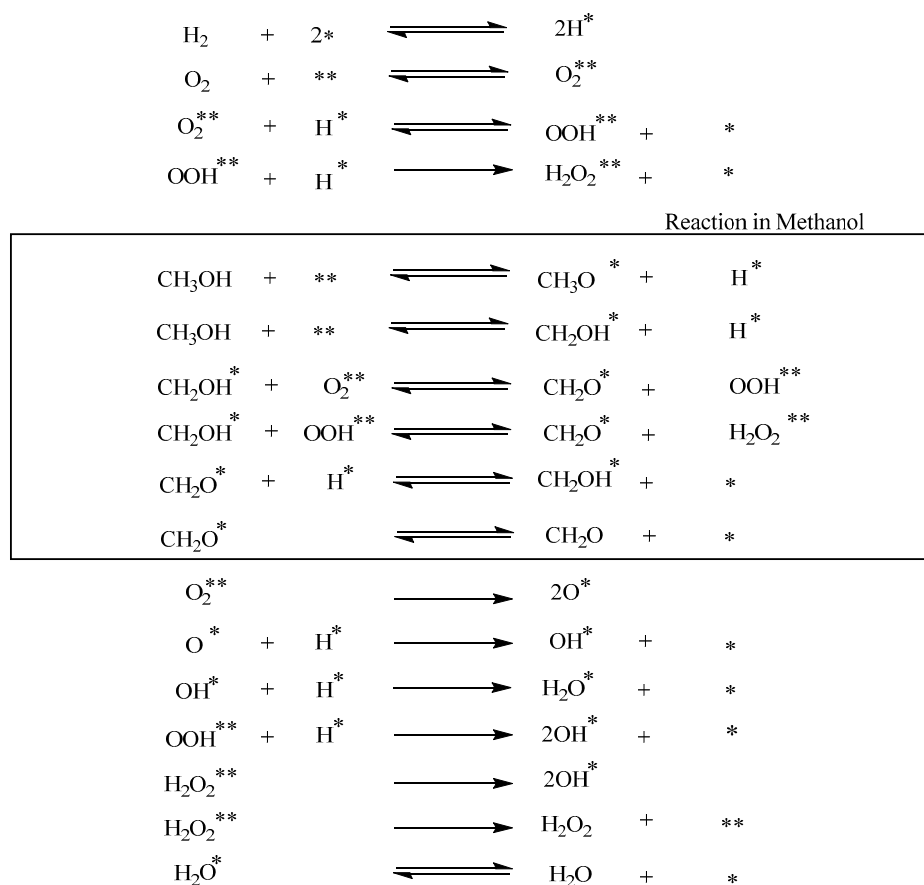
**Figure 6.** Transient behavior of peroxide and hydroxymethyl species.

Two conclusions can be drawn from these observations. Firstly, the formed methoxy species are not directly connected to the formation of hydrogen peroxide, in contrast to the hydroxymethyl species. This assumption is supported by the simultaneous rise of the hydroxymethyl species and the peroxide. Secondly, the following second maximum of the hydrogen peroxide signal and the decline of the hydroxymethyl signal indicate a consumption of the latter species during the formation of hydrogen. The rise of methoxy species during this consumption reveals the origin of the dehydrogenation products that are observed in the solvent and gas step experiments. These products are formed by the consumption of hydroxymethyl species during the formation of hydrogen peroxide during hydrogen deficiency, as observed in the gas step experiments.

Combining the knowledge gained from the FTIR-ATR experiments, the mechanism behind the oscillatory pattern is revealed to be closely related to the availability of hydrogen. During the first maximum, hydroxymethyl species are formed, thereby accelerating the formation of hydrogen peroxide. During this period, hydrogen is consumed in two processes. Firstly, the hydroxymethyl species are regenerated with available surface hydrogen, as indicated by the absence of dehydrogenation products, as well as the consumption of hydrogen in the classical ORR-mechanism. These processes consume hydrogen faster than the mass transfer of hydrogen from the gas phase to the catalyst surface, therefore limiting the availability of hydrogen on the surface. The second maximum is related to the formation of hydrogen peroxide in the hydrogen deficiency from hydroxymethyl species, thereby leading to the formation of the dehydrogenation products due to a lack of hydrogen for the regeneration and consumption of hydroxymethyl species, as observed in the FTIR-ATR experiments;



this is also due to a significant decrease in the concentration of hydrogen peroxide. After this minimum, the system stabilizes around a new steady state. From these observations, a reaction scheme is proposed, as displayed in Scheme 1. These results are similar to those independently observed by Flaherty et al. [28] in a semi-batch reactor. This further proves the very essential role of the solvent in the direct synthesis of hydrogen peroxide.



**Scheme 1.** Proposed reaction steps based on the solvent step FTIR-ATR experiments and the previous studies from the direct synthesis reaction in water with \* and \*\* representing free sites.

### 3. Experimental Section

#### 3.1. Materials

5% Pd/C-powder (Sigma-Aldrich, Espoo, Finland) was used as the catalyst as received. Methanol for HPLC (Sigma-Aldrich  $\geq 99.9\%$ ), ethanol (Altia Etax Aa  $\geq 99.5\%$ ), 2-propanol (Honeywell, Espoo, Finland  $\geq 99.5\%$ ) and deionized water ( $R = 16.9 \text{ M}\Omega\text{cm}$ ) were used as reaction media. All gases, namely  $\text{CO}_2$ ,  $5\% \text{H}_2/\text{CO}_2$ , and  $\text{O}_2$ , were supplied by AGA gas with 99.99% purity.

#### 3.2. Reactor Setup for the Experiments

The experiments were carried out in a co-current down-flow trickle bed reactor (TBR). This reactor setup allowed a flexible variation of temperature, solvent, gas feed and liquid residence time. The experimental set-up is shown schematically in Figure 7. The reactor was made of AISI 316 stainless steel, with a 30 cm length and a 1.5 cm inner diameter. To avoid decomposition of  $\text{H}_2\text{O}_2$  due to exposure to  $\text{Fe}^{3+}$  ions, the reactor was passivated with 40% nitric acid for 4 h. A maximum bed length of 20 cm can be accommodated in the reactor tube. To regulate the temperature, the reactor was fitted with a cooling coil connected to an external chiller (Grant LT D6G), which allows reaction temperatures between  $-20 \text{ }^\circ\text{C}$  and  $60 \text{ }^\circ\text{C}$ . The gases were fed via three independent mass flow controllers (MFC, Brooks's 5850 series). All MFCs were calibrated for actual mass flow with a digital

flowmeter (Humonics 520). The flow rates were calculated with mixture densities, which were calculated using the Soave–Redlich–Kwong equation of state with the Boston–Mathias modifications through Aspen Properties V10. A back pressure controller (Equilibar) was used to regulate and control the pressure in the reactor. Liquid was fed via a syringe pump (Eldex) which was fitted with a two-way valve to allow for switching between different solvents during the experiment. Gases and liquids were mixed in the upper part of the reactor system before the catalyst bed. The reactor temperature was controlled using a thermocouple (K-Type, Labfacility Ltd., Bognor Regis, UK) located directly in the catalyst bed. At the reactor outlet, the product stream could be directed either to the liquid waste or to a gas–liquid separator, consisting of a three-neck round-bottom flask from which liquid samples were taken via a peristaltic pump (Heidolph Pumpdrive 5206), and gas samples via a 100  $\mu\text{L}$  syringe. The piping system consisted of stainless steel AISI 316 with  $1/8$  inch size elements. In the reactor, the catalyst bed ( $\approx 0.5$  cm) was fitted between two plugs of glass wool. Downstream of the catalyst bed, quartz (Merck pro analysi) was used to locate the bed in the isothermal zone of the reactor. Quartz was used upstream to allow for mixing of the liquid and the gases. For safety reasons, the whole set-up was located in a fumehood equipped with a hydrogen sensor.

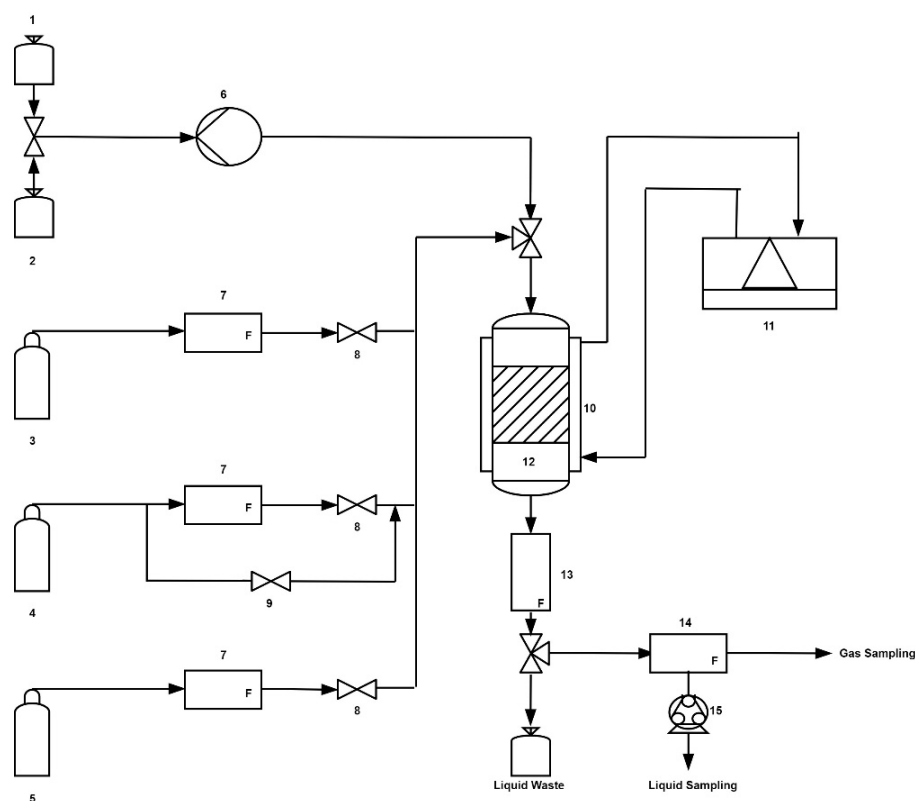


**Figure 7.** Schematic experimental apparatus. (1, 2) Solvent bottles, (3, 4, 5) gas bottles:  $\text{CO}_2$ ,  $5\% \text{H}_2/\text{CO}_2$ ,  $\text{O}_2$  (6) syringe pump, (7) mass flow controller (MFC), (8, 9) two-way valves for stopping the gas flow, (10) cooling coil, (11) thermostat, (12) trickle-bed reactor, (13) back pressure controller, (14) gas/liquid separator, (15) peristaltic pump.

### 3.3. Solvent Step Experiments

The solvent step experiments were carried out with 150 mg of 5 %Pd/C (catalyst powder mixed with 3 g of quartz) at  $P = 20$  bar,  $V_1 = 1 \text{ mL}\cdot\text{min}^{-1}$  and  $V_g = 4 \text{ mL}\cdot\text{min}^{-1}$ . All the experiments followed a similar procedure. Firstly, the loaded reactor was brought to a working pressure of 20 bar with  $\text{CO}_2$  and then exposed to the reaction gas mixture (4%  $\text{H}_2$ , 76%  $\text{CO}_2$ , 20%  $\text{O}_2$ ) for 1 h.  $\text{CO}_2$  has been proven before to enhance the direct synthesis with a combination of two main effects. The first is its tendency to form carbonic

acid. Acidic solutions are known to stabilize and enhance direct synthesis. In addition, CO<sub>2</sub> is known to significantly increase the volume of solutions under pressure, leading to higher concentrations after relaxation. These factors make CO<sub>2</sub> an attractive co-fed gas to enhance possible changes in concentrations after a solvent switch. [36,37] The liquid flow was started using pure water as the feed. The time at which the first droplet of liquid was visible at the outlet was marked as  $t_0$ . From then on, ca. 700  $\mu\text{L}$  of the liquid sample and 50  $\mu\text{L}$  of the gas samples were withdrawn every 20 min until 80 min. After this period, the feed was switched to the alcohol mixture, followed by a waiting period of 10 min; every 2 min, a sample was taken and analyzed. Each experiment was carried out three times. Following this procedure, three types of solvent step experiment were conducted:

Investigation of the influence of the alcohol concentration on the shape of the step response. For these experiments, the reaction temperature was fixed at 15 °C. Methanol was used as a model compound. To examine the influence of the alcohol concentration on the step shape, the experiments were carried out at three different concentrations of methanol: 10% in water, 50% in water and 100% were chosen, respectively.

Investigation of the influence of the temperature on the shape of the step response. The temperature effect was studied using methanol as the solvent. All chosen temperatures were kept low to minimize the potential influence of the product decomposition on the step shape. The experiments were carried out at 5 °C, 10 °C and 15 °C.

Investigation of the influence of the type of the alcohol on the step shape. To investigate the effect of different alcohols as potential reducing agents, alcohols with increasing substitution of the hydroxyl carbon were selected. For this reason, methanol, ethanol and 2-propanol were used in the experiments. During these experiments, the reaction temperature was 15 °C.

#### 3.4. Gas-Step Experiments

To investigate the effect of the surface concentrations of the gases on the reaction, gas-step experiments were applied. Similar conditions to those of the solvent step experiments prevailed. The general procedure was analogous to the solvent step experiments. After the pressure was reached, the dry catalyst was shortly exposed to one of the selected gases before the methanol feed was switched on. The gas feed was switched to the other gas after a variable time. The conducted experiments can be categorized two ways, as described below.

The influence of the surface concentration of oxygen on the reaction. Following the general procedure, the catalyst was exposed to 20% O<sub>2</sub> in CO<sub>2</sub> for 1 h with methanol, after which the gas mixture was changed to 5% H<sub>2</sub>/CO<sub>2</sub>. After the switch, a sample was withdrawn ( $\approx 500 \mu\text{L}$ ) in one minute intervals. The sampling period was varied based on the measured temperature of the catalyst bed, and the sampling was continued for at least 60 min.

The influence of the surface concentration of hydrogen on the reaction. In contrast to the corresponding experiments started with oxygen, the exposure time of the dry catalyst to 5% H<sub>2</sub> in CO<sub>2</sub> was varied time-wise. This is due to the fact that for hydrogen, significant differences were observable. The duration of the pre-treatment was varied from 15 min to 3 h. The sampling policy was identical to the previously described one.

#### 3.5. Sample Analysis

All samples were analyzed with two different methods of liquid chromatography. The concentration of hydrogen peroxide was determined with an HPLC (Agilent 1100 series) fitted with a UV-Vis-Detector. Some 15  $\mu\text{L}$  of a sample was injected into a reverse-phase (RP) column (Ultra Techsphere ODS 5u) with water ( $V = 0.5 \text{ mL} \cdot \text{min}^{-1}$ ) as the eluent at 40 °C. The detection was carried out at  $\lambda = 195.8 \text{ nm}$ , with references at  $\lambda = 360 \text{ nm}$  and  $\lambda = 100 \text{ nm}$ . To analyze the concentrations of the oxidation products of the alcohols, the liquid samples were analyzed with a separate RP-HPLC (HP 1100 series; Aminex HPX-87H). This method was based on a similar method published by Fatunmbi et.al [38], and modified to fit the

needs of the analysis. The gas samples were injected directly into the GC (Agilent 6980 N; HP-Plot Q and HP-Molsiv) with nitrogen as the carrier gas ( $V = 9.4 \text{ mL}\cdot\text{min}^{-1}$ ) at  $35 \text{ }^\circ\text{C}$ .

### 3.6. Deposition of the Catalyst on the ATR-Crystal

The catalyst suspension was prepared by mixing 1 mg of 5 %Pd/C (Aldrich) with 1 mL of pure ethanol (Altia Oy). The suspension was mixed with a Vortex and then sonicated for 30 min. Some 400  $\mu\text{L}$  of the catalyst suspension was then pipetted on to the crystal and subsequently air-dried at room temperature [27]. During the experiments, no leaching of the catalyst was observed.

### 3.7. FTIR-ATR Setup

All spectra were recorded on an IRTracer-100 (Shimadzu) spectrometer fitted with Harrick–Horizon optics and an MCT-Detector. The spectra were recorded every 10 s, producing an average of 10 scans with a resolution of  $8 \text{ cm}^{-1}$ , with unpolarized IR-radiation at an incident angle of  $65^\circ$  using a ZnSe-Crystal. The temperature of the ATR cells ( $l = 5 \text{ cm}$ ,  $w = 1 \text{ cm}$ ) was kept constant during the experiment. For the experiment, the cell was fed from four liquid reservoirs in which the solvent was saturated with  $\text{H}_2$  and  $\text{O}_2$ , respectively. As can be seen in Figure 8, the final reaction mixture could be freely determined by mixing the feed streams from different reservoirs pumped by two different peristaltic pumps (Ismatec Reglo Digital).

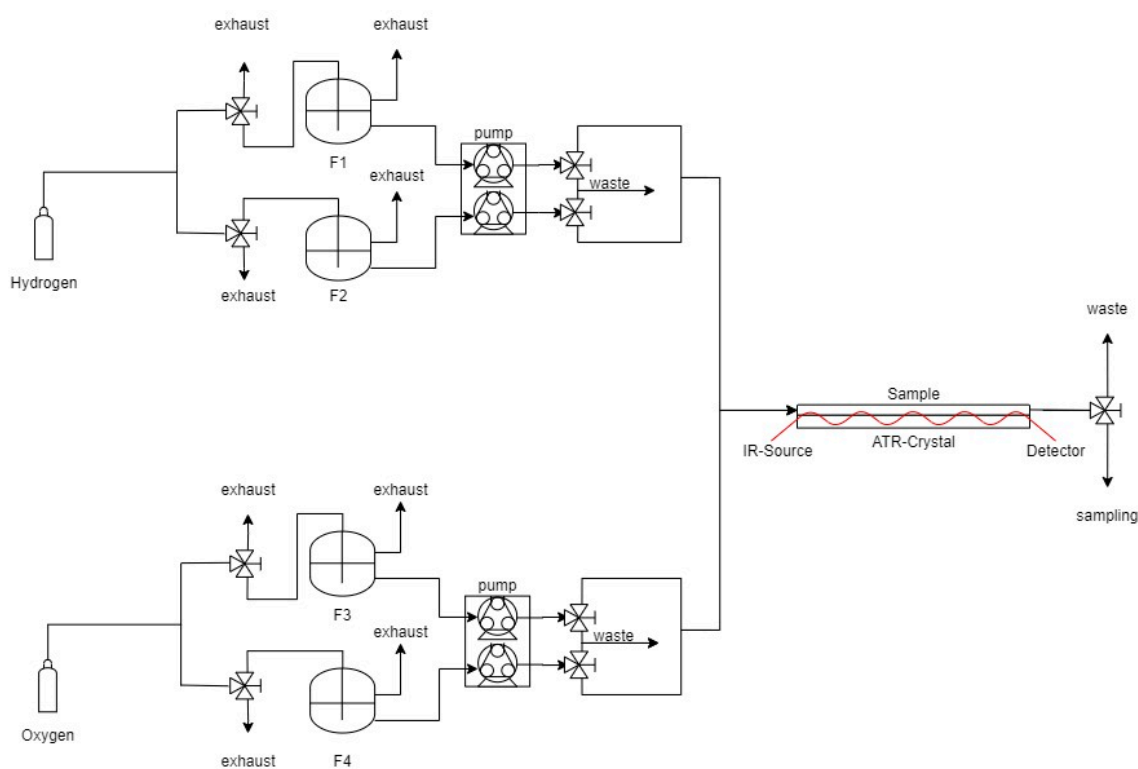


**Figure 8.** Flow scheme of the FTIR-ATR setup.

### 3.8. Solvent Step Experiments in ATR

The solvent step experiment consisted of two major parts. Firstly, the direct synthesis was performed in water. To achieve this, a flow of unsaturated water was applied through the ATR cell under reaction conditions ( $V = 0.2 \text{ mL}/\text{min}$ ;  $\vartheta = 15 \text{ }^\circ\text{C}$ ). Under these conditions, the background scan was recorded. After switching to a 1:1 mixture of  $\text{H}_2$ - and  $\text{O}_2$ -saturated water, the scanning began. After reaching the steady state in the presence water, the system was switched to the analogous system, using methanol as a solvent.

#### 4. Conclusions

In this work, we applied solvent step-change experiments in a laboratory-scale trickle bed reactor as well as in an in situ FTIR-ATR device to elucidate the reaction mechanism of the direct synthesis of hydrogen peroxide in methanol. In these experiments, similar transient responses for both setups were observed. Spectral reasons for these patterns were found. Based on these findings and existing knowledge of the mechanism in water, the previously proposed mechanism for methanol by Flaherty [28] was confirmed, and further confirmed for higher alcohols. This mechanism involves the transfer of protons from the alcohol to oxygen, in which the hydroxyalkyl formed acts as a co-catalyst which is regenerated with surface hydrogen. If the concentration of hydrogen is not sufficient, the hydroxyalkyl species react further to their corresponding carbonyl species.

**Supplementary Materials:** The following supporting information can be downloaded at: <https://www.mdpi.com/article/10.3390/catal13040753/s1>, Figure S1: TEM images of the purchased 5%Pd/C catalyst (Sigma-Aldrich); Figure S2: Particle size distribution of the purchased 5%Pd/C catalyst (Sigma-Aldrich); Figure S3: Proof of reproducibility of the transient response of the hydrogen peroxide concentration after the switch from water to 10% methanol in water; Figure S4: Proof of reproducibility of the transient response of the hydrogen peroxide concentration after the switch from water to 50% methanol in water; Figure S5: Proof of reproducibility of the transient response of the hydrogen peroxide concentration after the switch from water to 100% methanol in water.; Figure S6: Time dependency of the observed FTIR-Spectra during the solvent switch from water to methanol; Figure S7: Spectrum after the switch from water to methanol. (TOS = 7780 s).

**Author Contributions:** Conceptualization, O.R. and T.S.; methodology, O.R. and K.E.; software, O.R.; validation, O.R., K.E. and T.S.; formal analysis, O.R.; investigation, O.R.; resources, O.R.; data curation, O.R.; writing—original draft preparation, O.R.; writing—review and editing, O.R. and T.S.; visualization, O.R.; supervision, T.S.; project administration, T.S.; funding acquisition, T.S. All authors have read and agreed to the published version of the manuscript.

**Funding:** This work is part of the activities financed by the Academy of Finland through the Academy Professor's grants 319002 (T. Salmi), 320115 and 345053 (O. Reinsdorf). The economic support of the Academy of Finland is gratefully acknowledged.

**Data Availability Statement:** The data that support the findings of this study are available from the corresponding author upon reasonable request.

**Conflicts of Interest:** The authors declare no conflict of interest.

#### References

1. Goor, G.; Glenneberg, J.; Jacobi, S.; Dadabhoy, J.; Candido, E. *Hydrogen Peroxide*. *Ullmann's Encyclopedia of Industrial Chemistry Weinheim*; Wiley: Hoboken, NJ, USA, 2019.
2. Samanta, C.; Choudhary, V.R. Direct oxidation of H<sub>2</sub> to H<sub>2</sub>O<sub>2</sub> over Pd/Ga<sub>2</sub>O<sub>3</sub> catalyst under ambient conditions: Influence of halide ions added to the catalyst or reaction medium. *Appl. Catal. A Gen.* **2007**, *326*, 28–36. [[CrossRef](#)]
3. Wilson, N.M.; Priyadarshini, P.; Kunz, S.; Flaherty, D.W. Direct synthesis of H<sub>2</sub>O<sub>2</sub> on PdZn nanoparticles: The impact of electronic modifications and heterogeneity of active sites. *J. Catal.* **2018**, *357*, 163–175. [[CrossRef](#)]
4. Ntainjua, E.; Piccinini, M.; Pritchard, J.C.; Edwards, J.K.; Carley, A.F.; Moulijn, J.A.; Hutchings, G.J. Effect of halide and acid additives on the direct synthesis of hydrogen peroxide using supported gold-palladium catalysts. *ChemSusChem* **2009**, *2*, 575–580. [[CrossRef](#)] [[PubMed](#)]
5. Li, J.; Yoshizawa, K. Mechanistic aspects in the direct synthesis of hydrogen peroxide on PdAu catalyst from first principles. *Catal. Today* **2015**, *2481*, 42–148.
6. Wilson, N.M.; Flaherty, D.W. Mechanism for the Direct Synthesis of H<sub>2</sub>O<sub>2</sub> on Pd Clusters: Heterolytic Reaction Pathways at the Liquid–Solid Interface. *J. Am. Chem. Soc.* **2016**, *138*, 574–586. [[CrossRef](#)]
7. Flaherty, D.W. Direct Synthesis of H<sub>2</sub>O<sub>2</sub> from H<sub>2</sub> and O<sub>2</sub> on Pd Catalysts: Current Understanding, Outstanding Questions, and Research Needs. *ACS Catal.* **2018**, *8*, 1520–1527. [[CrossRef](#)]
8. Paunovic, V.; Ordonsky, V.V.; Sushkevich, V.L.; Schouten, J.C.; Nijhuis, T.A. Direct Synthesis of Hydrogen Peroxide over Au-Pd-Catalyst—The Effect of Co-Solvent Addition. *ChemCatChem* **2015**, *7*, 1161–1176. [[CrossRef](#)]
9. Han, Y.; Lunsford, J.H. Direct formation of H<sub>2</sub>O<sub>2</sub> from H<sub>2</sub> and O<sub>2</sub> over a Pd/SiO<sub>2</sub> catalyst: The roles of the acid and the liquid phase. *J. Catal.* **2005**, *230*, 313–316. [[CrossRef](#)]

10. Gallina, G.; García-Serna, J.; Salmi, T.O.; Canu, P.; Biasi, P. Bromide and Acids: A Comprehensive Study on Their Role on the Hydrogen Peroxide Direct Synthesis. *Ind. Eng. Chem. Res.* **2017**, *56*, 13367–13378. [[CrossRef](#)]
11. Burch, R.; Ellis, P.R. An investigation of alternative catalytic approaches for the direct synthesis of hydrogen peroxide from hydrogen and oxygen. *Appl. Catal. B Environ.* **2003**, *42*, 203–211. [[CrossRef](#)]
12. Liu, Q.; Lundsford, J.H. Controlling factors in the direct formation of H<sub>2</sub>O<sub>2</sub> from H<sub>2</sub> and O<sub>2</sub> over a Pd/SiO<sub>2</sub> catalyst in ethanol. *Appl. Catal. A Gen.* **2006**, *314*, 94–100. [[CrossRef](#)]
13. Liu, Q.; Gath, K.K.; Bauer, J.C.; Schaak, R.E.; Lunsford, J.H. The Active Phase in the Direct Synthesis of H<sub>2</sub>O<sub>2</sub> from H<sub>2</sub> and O<sub>2</sub> over Pd/SiO<sub>2</sub> Catalyst in a H<sub>2</sub>SO<sub>4</sub>/Ethanol System. *Catal. Lett.* **2009**, *132*, 342–348. [[CrossRef](#)]
14. Gemo, N.; Biasi, P.; Canu, P.; Salmi, T.O. Mass transfer and kinetics of H<sub>2</sub>O<sub>2</sub> direct synthesis in a batch slurry reactor. *Chem. Eng. J.* **2012**, *207–208*, 539–551. [[CrossRef](#)]
15. Salmi, T.O.; Gemo, N.; Biasi, P.; Serna, J.G. Product distribution analysis of the hydrogen peroxide direct synthesis in an isothermal batch reactor. *Catal. Today* **2015**, *248*, 108–114. [[CrossRef](#)]
16. Biasi, P.; Menegazzo, F.; Pinna, F.; Eränen, K.; Canu, P.; Salmi, T.O. Hydrogen Peroxide Direct Synthesis: Selectivity Enhancement in a Trickle Bed Reactor. *Ind. Eng. Chem. Res.* **2010**, *49*, 10627–10632. [[CrossRef](#)]
17. Biasi, P.; Canu, P.; Menegazzo, F.; Pinna, F.; Salmi, T.O. Direct synthesis of hydrogen peroxide in a trickle bed reactor: Comparison of Pd-based catalysts. *Ind. Eng. Chem. Res.* **2012**, *51*, 8883–8890. [[CrossRef](#)]
18. Biasi, P.; Menegazzo, F.; Pinna, F.; Eränen, K.; Salmi, T.O.; Canu, P. Continuous H<sub>2</sub>O<sub>2</sub> direct synthesis over PdAu catalysts. *Chem. Eng. J.* **2011**, *176–177*, 172–177. [[CrossRef](#)]
19. Bennett, C.O. Experiments and processes in the transient regime for heterogeneous catalysis. *Adv. Catal.* **1999**, *44*, 329–416.
20. Bennett, C.O. The Transient Method and Elementary Steps in Heterogeneous Catalysis. *Catal. Rev. Sci. Eng.* **1976**, *13*, 121–148. [[CrossRef](#)]
21. Kobayashi, H.; Kobayashi, M. Transient response method in heterogeneous catalysis. *Catal. Rev. Sci. Eng.* **1974**, *10*, 139–176. [[CrossRef](#)]
22. Biloen, P. Transient kinetic methods. *J. Mol. Catal.* **1983**, *21*, 17–24. [[CrossRef](#)]
23. Hind, A.R.; Bhargava, S.K.; McKinnon, A. At the solid/liquid interface: FTIR/ATR—The tool of choice. *Adv. Colloid Interface Sci.* **2001**, *93*, 91–114. [[CrossRef](#)] [[PubMed](#)]
24. Zhang, H.X.; Wang, S.H.; Jiang, K.; André, T.; Cai, W.B. In situ spectroscopic investigation of Co accumulation and poisoning on Pd black surfaces in concentrated HCOOH. *J. Power Sources* **2012**, *199*, 165–169. [[CrossRef](#)]
25. Keresszegi, C.; Ferri, D.; Mallat, T.; Baiker, A. On the role of CO formation during the aerobic oxidation of alcohols on Pd/Al<sub>2</sub>O<sub>3</sub>: An in situ attenuated total reflection infrared study. *J. Catal.* **2005**, *234*, 64–75. [[CrossRef](#)]
26. Garrigues, J.M.; Perez-Ponce, A.; Garrigues, S.; de la Guardia, M. Direct determination of ethanol and methanol in liquid samples by means of vapor phase-Fourier transform infrared spectroscopy. *Vib. Spectrosc.* **1997**, *15*, 219–228. [[CrossRef](#)]
27. Feng, L.; Wei, J.; Reisler, H. Rotationally Resolved Infrared Spectroscopy of the Hydroxymethyl Radical (CH<sub>2</sub>OH). *J. Phys. Chem. A* **2004**, *108*, 7903–7908. [[CrossRef](#)]
28. Adams, J.S.; Chemburkar, A.; Priyadarshini, P.; Ricciardulli, T.; Lu, Y.; Maliekkal, V.; Sampath, A.; Winikoff, S.; Karim, A.; Neurock, M.; et al. Solvent molecules form surface redox mediators in situ and cocatalyze O<sub>2</sub> reduction on Pd. *Science* **2021**, *371*, 626–632. [[CrossRef](#)]
29. Nayak, S.; Biedermann, P.U.; Stratmann, M.; Erbe, A. A mechanistic study of the electrochemical oxygen reduction on the model semiconductor n-Ge (100) by ATR-IR and DFT. *Phys. Chem. Chem. Phys.* **2012**, *15*, 5771. [[CrossRef](#)]
30. Gates, J.A.; Kesmodel, L.L. Methanol adsorption and decomposition on clean and oxygen precovered palladium (111). *J. Catal.* **1983**, *83*, 437–445. [[CrossRef](#)]
31. Redington, R.L.; Olson, W.B.; Cross, P.C. Studies of hydrogen peroxide: The infrared spectrum and the internal rotation problem. *J. Chem. Phys.* **1962**, *36*, 1311. [[CrossRef](#)]
32. Zeglinski, J.; Piotrowski, G.P.; Piekos, R. A study of interaction between hydrogen peroxide and silica gel by FTIR spectroscopy and quantum chemistry. *J. Mol. Struct.* **2006**, *794*, 83–91. [[CrossRef](#)]
33. Vacquea, V.; Sombre, B.; Huvennea, J.P.; Legrand, P.; Such, S. Characterisation of the O-O peroxide bond by vibrational spectroscopy. *Spectrochim. Acta Part A* **1997**, *53*, 55–66.
34. Schauermaun, S.; Hoffmann, J.; Johánek, V.; Hartmann, J.; Libuda, J. Adsorption, decomposition and oxidation of methanol on alumina supported palladium particles. *Phys. Chem. Chem. Phys.* **2002**, *4*, 3909–3918. [[CrossRef](#)]
35. Wu, J.B.; Shi, R.P.; Qin, Z.F.; Huan, L.I.; Li, Z.K.; Zhu, H.Q.; Zhao, Y.X.; Wang, J.G. Selective oxidation of methanol to methyl formate over bimetallic Au-Pd nanoparticles supported on SiO<sub>2</sub>. *J. Fuel Chem. Technol.* **2019**, *47*, 780–790. [[CrossRef](#)]
36. García-Serna, J.; Moreno, T.; Biasi, P.; Cocero, M.J.; Mikkola, J.-P.; Salmi, T.O. Engineering in direct synthesis of hydrogen peroxide: Targets, reactors and guidelines for operational conditions. *Green Chem.* **2014**, *16*, 2320. [[CrossRef](#)]
37. Jessop, P.G.; Subramaniam, B. Gas-Expanded Liquids. *Chem. Rev.* **2007**, *107*, 2666–2694. [[CrossRef](#)] [[PubMed](#)]
38. Fatunmbi, H.; Fatunmbi, B. HPLC Separation Analyses of Peroxyacetic acid and acetic acid coexisting with hydrogen peroxide in the equilibrium mixture. *SMT Sep. J.* **2017**, *1*, 1–3.

**Disclaimer/Publisher's Note:** The statements, opinions and data contained in all publications are solely those of the individual author(s) and contributor(s) and not of MDPI and/or the editor(s). MDPI and/or the editor(s) disclaim responsibility for any injury to people or property resulting from any ideas, methods, instructions or products referred to in the content.